Design proposal for two poles lattice filter of and MZI interferometer

Edx Username: Silman

ABSTRACT The attached proposal is a requirement for completion of an online Edx course: *"**Silicon Photonics Design, Fabrication and Data Analysis**" (Jan-Mar. 2021)*. The proposal contains the simulation, analysis and experimental results of some basic passive photonic integrated circuit devices, namely, unbalanced Mach Zehnder Interferometers (MZI)s and a second order lattice filter. I explore the device variation through Monte Carlo analysis, where it shows that for MZI the wafer variations characterized through thickness and height, causes some shift in the response, along with slight degradation in insertion loss. However, for lattice filter such variations results in a significant performance degradation, which is the reason I kept two designs with the same dimension on my allocated floorplan.

INDEX TERMS Photonic Integrated Circuits. Lattice filters. Mach Zehnder Interferometer.

I. INTRODUCTION

With the ever-growing demand of high speed data transmission and processing, photonic integrated circuits (PIC)s form an indispensable platform in the modern technology [1]. Not only for data processing, but PICs are also one of the popular methods used for biosensing [2], offering new trends in diagnosis for the medical community. Notably, related to our time being, a big portion of funds are devoted to Covid-19 biosesing research based on Silicon Photonics[3]. There are indeed enormous amount applications based PIC that would not be available using the conventional microelectronics industry, e.g., cryogenic PICs for quantum applications[4] Lidar system in automotive industry[5], optical gyroscope for space applications [6], , … an interested reader can refer to [7] for further applications.

In this report however, I focus on PICs related to data processing, namely, Mach Zehnder interferometers, and lattice filters for optical communications. In Section II I present the basic building blocks for the devices, then in Section III, I present the design for the MZI and its layout results. In Section IV, I present the lattice filter of second order design and its layout results.

II. Basic Building Blocks

Based on a single etch fabrication process available in this course, all the basic building blocks should have SiO2 substrate, and 220 nm Silicon to be patterned. In my work the basic building blocks are:

1. TE straight waveguide of width 500nm and height 220nm.
2. TE Bend waveguide of radius 5um.
3. Broadband directional coupler from EBeam PDK provided in that course[8].
4. Optimized Y branch from EBeam PDK provided in that course [9].

These building blocks are used in simulations as interconnects, where the compact models are already provided.

A. Straight TE Waveguide 1550nm

The inset of Fig.1a shows the straight Waveguide (WG) used in this work, it has SiO2 substrate, and also will be cladded by a SiO2 layer (not shown here for clarity). I use Lumerical Mode solution to get the effective index of the TE0 mode, as shown in Fig. 1a. This effective index (n_{eff}) can be fitted to create a compact model for the straight WG, and then can be used in Lumerical interconnect simulation without further Finite Difference Time Domain (FDTD) simulation. The fit curve takes the general formula of,

$$n_{eff} = n_0 + \sum_{m=1}^{\infty} n_m \, (\lambda - \lambda_0)^m \qquad (1)$$

Where we choose $\lambda_0 = 1550$nm. Indeed due to the smooth behavior of n_{eff} versus λ we can have two terms only from the series in (1), i.e. up to m=2. I use the provided fit algorithm in the course to find the coefficients,n_0, n_1 and n_2. The effective index is written as,

$$n_{eff} = 2.447 - 1.133(\lambda - \lambda_0) - 0.044(\lambda - \lambda_0)^2 \qquad (2)$$

This curve is plotted against the actual retrieved data as shown in Fig. 1a to confirm its validity to represent the effective index in this range. Finally, I plot the mode profile (the energy distribution) inside the TE0 mode as shown in the upper right inset in Fig. 1a where it shows that most of the energy reside inside the waveguide

cross section. I additionally calculated the group index n_g as shown in Fig. 1b, where it shows that a value of 4.2 can be used for further calculations as will be shown in the results sections.

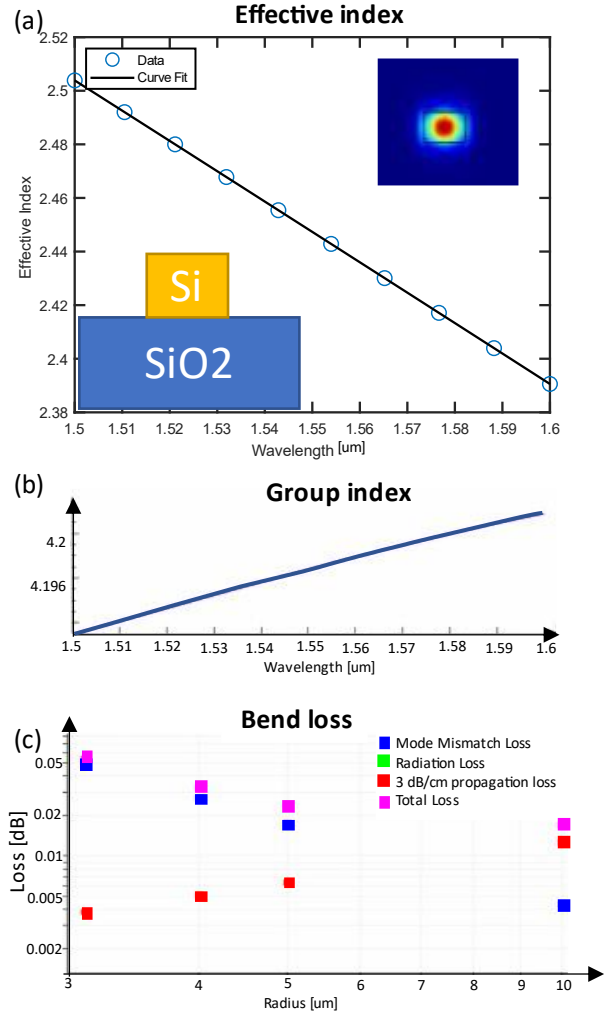

FIG. 1. (a) Effective index of the TE0 mode in Si WG (width= 500nm and height=220 nm) from Mode solution and fitted using the Eq (1). (b) Calculated group index of the same mode. (c) Characterization of the various types of the bend loss for the same mode when the WG is bent to form a circle.

B. Bend TE Waveguide 1550nm

To route the optical mode easily between different components, bend of WG is necessary. The bend is a source of increased loss during the mode propagation, and there are mainly three significant types of loss are present. The mode mismatch loss, that is attributed to mismatch between the two connected straight WG at the bend terminals, which is the main source of losses for smaller radius < 5um as shown in Fig. 1c. The 3dB/cm increases with increasing the bend radius and become more significant at radius > 5um. This 3dB/cm loss is an experimental estimation for the fabrication errors, i.e., rough side walls of the waveguide, or imperfection in the WG width or height along the mode path. The radiation loss is very small comparable to other losses, and therefore in the range of losses printed in Fig. 1c, this loss does not appear. Thus we conclude that an optimum bend radius for TE0 mode is something between 5-8um. In this report I use 5um as the default bend radius.

C. broadband directional coupler (bdc)

I use a wideband directional coupled from the provided PDK, and can be found in [8]. The basic idea of broadband response is to use asymmetric WG sections to compensate for the wavelength depend coupling ratio.

The wideband direction coupler can obtain coupling ratios from 1% to 99% within band of 100nm starting at 1500nm. To obtain the desired coupling ratio, I used 2 bdc back to back with phase cancellation technique in [8]. For example, Fig. 2a shows the simulation result of the PDK version of the bdc to obtain coupling of 10% coupling, where the dimensions are plotted in the figure. Fig. 2b on the other hand shows the calculated transmission to port 3 (coupled) and port 4 (through).

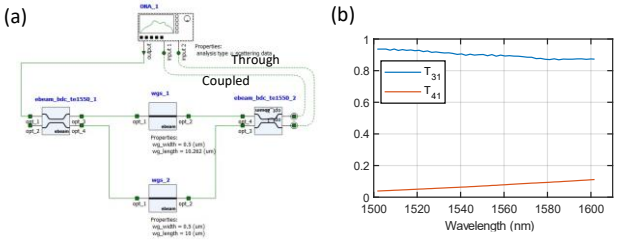

FIG. 2. (a) Lumerical interconnect setup to obtain any desired coupling ratio. (b) example for 10%-90% coupler at 1550nm.

D. Optimized Y-branch

I use Y-branch provided in the PDK, based on particle swarm optimization [9]. The response of the Y-branch for an input excitation is shown in Fig. 3, where it confirms the broadband operation of the splitter.

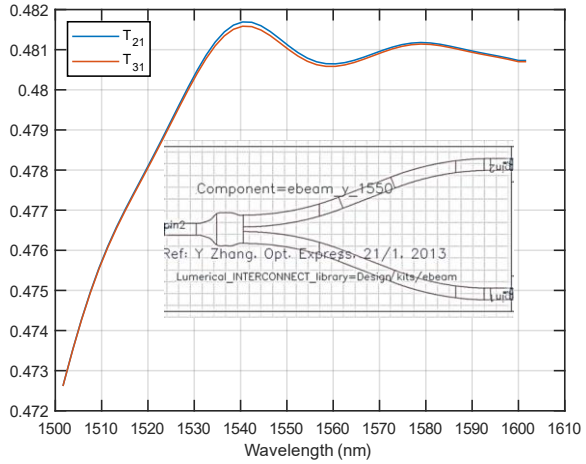

FIG. 3. Response of Y branch from [9].

III. MZI Designs in EBeam_Silman.gds

Provided in EBeam_Silman.gds, I have two types of designs, MZI interferometers (three different designs) in this Section and 2nd order lattice filters (two identical designs) in Section (IV).

A prototype of an MZI in the gds file is shown in Fig. 4a, where we have fiber grating coupler (GC) for the input and output, and two Y splitters, each connected to a GC, and each branch of the Y splitter is connected to the other branch on the other Y splitter, where these connections are of different length forming the ΔL in the MZI equation,

$$I = I_{in}(1 + \cos \beta \Delta L) \quad (3)$$

where, $\beta = 2\pi/\lambda_0\, n_g$, and n_g is the group index. The free spectral range FSR is defined as the spectral distance between two peaks in I and is evaluated as,

$$FSR = \lambda_0^2/(n_g \Delta L) \quad (4)$$

A. MZI13nm

The proposed MZI is a simple unbalanced MZI, with difference in length of 41um. The layout is shown in Fig. 4a, and the simulated response is shown in 4b. Based on Eq. (3) and using, $n_g = 4.2$ as derived from Fig. 1, we estimate theortically FSR=13.9nm at 1550nm which is indeed the same value as shown in Fig.4b.

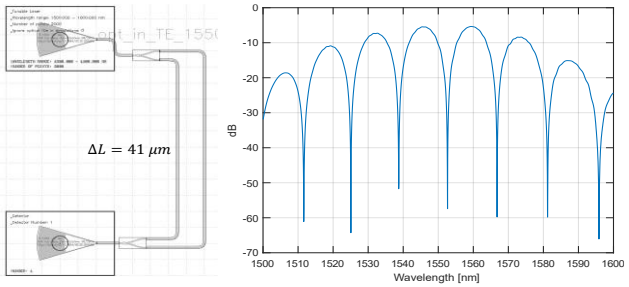

FIG. 4. (a) Typical MZI layout. (b) Transmission spectra in dB for $\Delta L = 41\mu m$.

B. MZI5nm

Another MZI with $\Delta L = 117.5\mu m$, in Fig. 5a, theoretically FSR=5nm at 1550nm as shown similar to the simulated value in Fig. 5 which is indeed the same value as shown in Fig.5b.

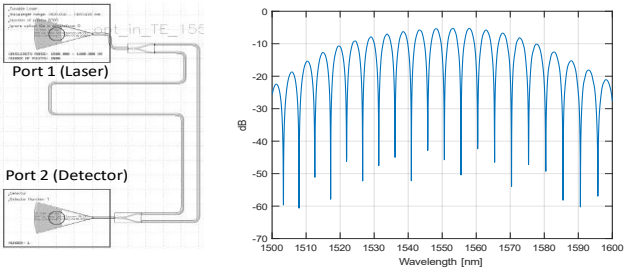

FIG. 5. (a) layout of MZI. (b) Transmission spectra in dB for $\Delta L = 117.5\mu m$.

C. MZI13nm3dB

In order to get familiar with more passive components (bdc, Y splitter), I also have a more complicated MZI as shown in Fig. 6a with $\Delta L = 191\mu m$. The theortical FSR is 3nm, which is in close agreement with simulations as shown in Fig. 6b.

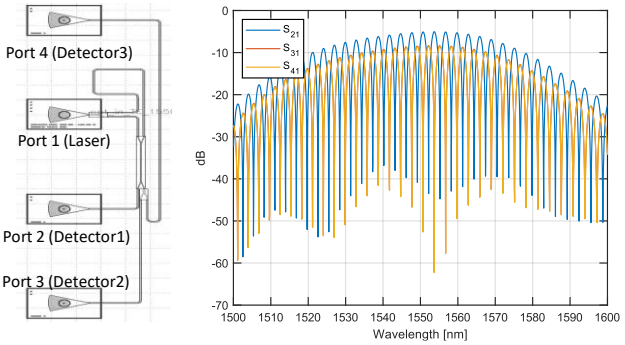

FIG. 6. (a) layout of MZI. (b) Transmission spectra in dB for $\Delta L = 191\mu m$ at port 2, 3 and 4.

Finally, Table 1 shows the calculated ΔL for each MZI, and the FSR.

Name of MZI	MZI13nm	MZI5nm	MZI13nm3dB
ΔL	$41\mu m$	$117.5\mu m$	$191\mu m$
FSR	$14nm$	$5nm$	$3nm$

Additionally, I have performed Mont Carlo simulation for possible shift in the FSR. The Monte Carlo simulation parameters are (Wafer to Wafer Variation):

1. Standard deviation (s.t.d.) = 5nm for width.
2. s.t.d = 3nm for thickness.
3. Number of test wafers=10

The results for device, "MZI13nm is shown in Fig. 7 where it shows that a s.t.d. of 0.386nm is expected for the given Monte Carlo parameters.

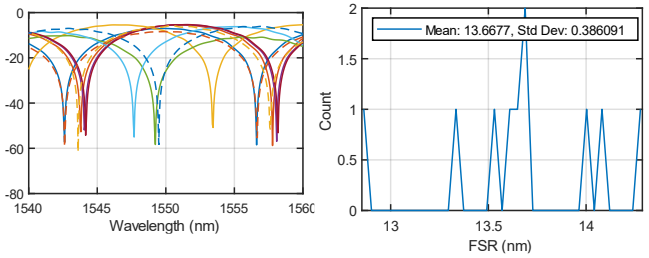

FIG. 7 (a) Variations of the transmission spectral response for 10 Monte Carlo simulation runs. (b) FSR range variations count.

IV. Lattice filter Design in EBeam_Silman.gds

The interesting idea of implementing filters based on systematic iterations is very powerful for design acceleration. Optical half -band filter is presented in [10] and can produce flat band filter with high rejection ratio of any desired filter

order. Increasing the order means increase similar stage, but with different, yet known, values. Unfortunately, a filter implementation based on this idea is very sensitive to any variations in length, width or heigh. Therefore, the simplest approach to follow is to fabricate many identical filter, hopefully we can get the desired filter response. Unfortunately, for the allocated floorplan space, the maximum number of filters I was able to put is just 2. So it would be very surprising if I got some working filter, at least for some bandwidth.

The designed filter is a 2nd order filter with the coupling coefficients and the length difference are initially set as given in Table 1 in [10], are then optimized to get the desired response. The filter layout is too difficult to show in one figure in this report, so I recommend opening it from the attached EBeam_Silman.gds file. Fig. 8 instead shows the response after many optimization to reach the best result. Indeed it shows that an average rejection of 17dB and bandwidth of 15nm around 1550nm.

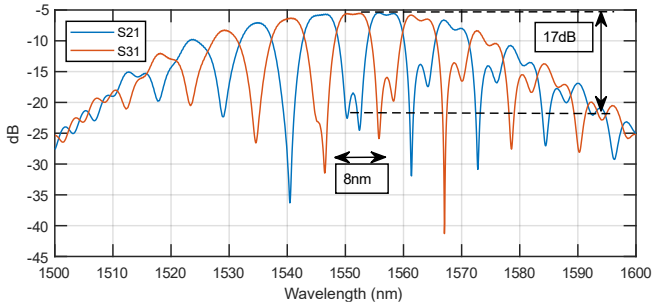

FIG. 8 response of 2nd order lattice filter based on [10].

To confirm the sensitivity of the design, I performed Monte Carlo simulation with 5 varaitions, with the same properties in Sec. III (c). The filter response quickly deteoriate that even I can not see any acceptable response as shown in Fig. 9

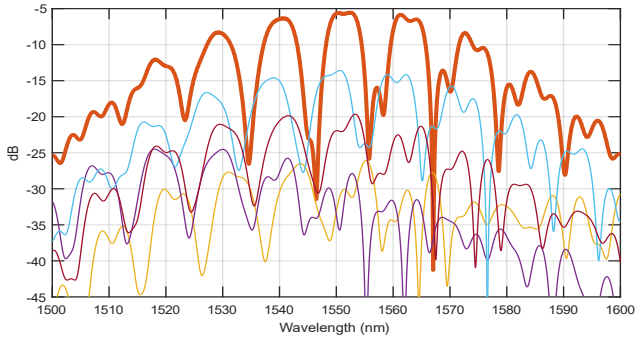

FIG. 9 Monte Carlo simulation results for 5nm std in width and 3nm std in height.

V. CONCLUSION

In summary, the report has proposed the post layout simulation results for passive components, namely MZI, and lattice filter. The derived group index from the FSR equation of the MZI connects well with the one obtained from simulation with a little deviation at smaller wavelength. I also presented the results for 2nd order filter, with bandwidth of 6nm and an average rejection of 17dB around 1550nm. The Monte Carlo simulation results, shows that the response to MZI is minimal, with shift in its spectral response, or slight degradation in loss. However, the same parameters for Monte Carlo simulation shows that the filter response is very sensitive to any variations in the wafer.

REFERENCES

[1] Chrostowski, L. and Hochberg, M., 2019. *Silicon photonics design*. Cambridge: Cambridge University Press.

[2] Iqbal, M., Gleeson, M.A., Spaugh, B., Tybor, F., Gunn, W.G., Hochberg, M., Baehr-Jones, T., Bailey, R.C. and Gunn, L.C., 2010. Label-free biosensor arrays based on silicon ring resonators and high-speed optical scanning instrumentation. *IEEE Journal of selected topics in quantum electronics*, *16*(3), pp.654-661.

[3] Patricia Daukantas, "Chasing COVID-19 with Photonics", article in Optics & Photonics found at, https://www.osa-opn.org/home/newsroom/2020/september/chasing_covid-19_with_photonics/.

[4] Chakraborty, U., Carolan, J., Clark, G., Bunandar, D., Gilbert, G., Notaros, J., Watts, M.R. and Englund, D.R., 2020. Cryogenic operation of silicon photonic modulators based on the DC Kerr effect. *Optica*, *7*(10), pp.1385-1390.

[5] Li, Y. and Ibanez-Guzman, J., 2020. Lidar for autonomous driving: The principles, challenges, and trends for automotive lidar and perception systems. *IEEE Signal Processing Magazine*, *37*(4), pp.50-61.

[6] Ezekiel, S., 2006, October. Optical gyroscope options: principles and challenges. In *Optical Fiber Sensors* (p. MC1). Optical Society of America.

[7] Dong, P., Chen, Y.K., Duan, G.H. and Neilson, D.T., 2014. Silicon photonic devices and integrated circuits. *Nanophotonics*, *3*(4-5), pp.215-228.

[8] Lu, Z., Yun, H., Wang, Y., Chen, Z., Zhang, F., Jaeger, N.A. and Chrostowski, L., 2015. Broadband silicon photonic directional coupler using asymmetric-waveguide based phase control. *Optics express*, *23*(3), pp.3795-3808.

[9] Zhang, Y., Yang, S., Lim, A.E.J., Lo, G.Q., Galland, C., Baehr-Jones, T. and Hochberg, M., 2013. A compact and low loss Y-junction for submicron silicon waveguide. *Optics express*, *21*(1), pp.1310-1316.

[10] Jinguji, K. and Oguma, M., 2000. Optical half-band filters. *Journal of lightwave technology*, *18*(2), p.252.